Published in the Proceedings of the International Offshore and Polar Engineering Conference
2016-January (pp.1363-1370)

An Efficient Coupled-Mode/FEM Numerical Method for Linear Wave Propagation Over 3D Variable Bathymetry Domains

Theodosios K. Papathanasiou[1], Angeliki E. Karperaki[2], Kostas A. Belibassakis[2]

[1]Dipartimento di Ingegneria Civile, Ambientale e Meccanica, University of Trento, Trento, Italy.

[2]School of Naval Architecture and Marine Engineering, National Technical University of Athens, Athens, Greece.

ABSTRACT

A robust numerical algorithm for the simulation of linear water wave propagation over uneven bottom topography is developed. The solution strategy is based on a highly efficient reduction of the 3D problem to a system of partial differential equations by means of a consistent coupled mode series expansion for water wave propagation over variable seabed. The main feature of the proposed series representation is the incorporation of special terms in the vertical expansion basis, accounting for the bottom boundary condition of the varying seabed. The formulation of the 2D system follows from the variations, with respect to the expansion coefficients (functions of the horizontal plane spatial coordinates), of a suitably chosen energy functional. The resulting model is a variable coefficient system of second order, with respect to the spatial coordinates, Partial Differential Equations (PDEs). Linear triangular finite elements are employed for the solution of this PDE system offering flexibility in the discretization of complex 2D domains. The numerical method developed has been applied to several test cases yielding accurate representations of the wave field at relatively low computational cost and small execution times.

KEY WORDS: Water Waves; Variable Bathymetry; Coupled Mode Systems; Finite Elements; Transient Analysis.

INTRODUCTION

Water wave propagation in complex three dimensional domains, characterised by variable seabed topography, is a subject of both theoretical and practical significance (Stoker, 1957; Dingemans, 1997). In the case of shallow water conditions, Boussinesq type approximation models have been established and widely used (e.g. Beji & Battjes, 1994; Madsen et al (2006)). For intermediate depths however, where the effects of the surface gravity wave – seabed interactions (e.g. shoaling) are still significant, the aforementioned models are not appropriate. A disadvantage of Boussinesq- type approximations is that the vertical structure of the wavefield is given by a chosen function, hence failing to account for abrupt changes in bathymetry or the presence of localised scatterers. Massel (1993) presented an extended version of the mild-slope equations, where the vertical structure or the wavefield is given by a local-mode series representation. However, the standard spectral representation for the wave potential is not consistent with the Neumann condition on the sloping seabed boundary. In order to remedy this inconsistency an enhanced coupled mode series expansion for water wave propagation over variable seabed was introduced by Belibassakis & Athanassoulis (2006, 2011). The main feature of the proposed series representation is the incorporation of special terms in the vertical expansion basis, accounting for the bottom boundary condition at the varying seabed and the boundary condition on the free surface. The particular representation of the wave potential has been proven to be rapidly convergent and typically only a few modes are sufficient to yield very accurate approximations of the three dimensional field.

Published in the Proceedings of the International Offshore and Polar Engineering Conference
2016-January (pp.1363-1370)

In the present work, a robust numerical algorithm for the simulation of linear water wave propagation over uneven bottom topography is developed. The consistent coupled mode series expansion for the wave potential (Belibassakis & Athanassoulis, 2006; 2011) is adopted. The formulation of the 2D system follows from the variations, with respect to the expansion coefficients, of Luke's functional. The resulting model is a variable coefficient system of second order, with respect to the spatial coordinates, Partial Differential Equations (PDEs). Linear triangular finite elements are employed for the solution of this system offering flexibility in the discretization of complex 2D domains. Nodal unknowns are the velocity potential coefficients of the modal expansion series and the free surface elevation. Since all derivatives up to second order are present in the system differential operator, a nonconforming approach for the stiffness integral calculations is adopted. The variable PDE coefficients are calculated at the barycentre of each element and one point quadrature is adopted. This selection reduces the computational cost, while the error introduced by the low order integration rule is insignificant for the selected approximation order, as the finite element mesh becomes finer. The numerical method developed has been applied to several test cases yielding accurate representations of the wave field at relatively low computational cost and small execution times.

LINEAR GRAVITY WAVE PROPAGATION MODEL

In this section, the linear Cauchy-Poisson problem for water wave propagation over variable bathymetry domains will be briefly presented. Given a scalar function $b(x,y):\Omega\subset\mathbb{R}^2\to\mathbb{R}_+$, an inviscid, incompressible fluid is assumed to occupy domain

$$D=\left\{(x,y)\in\Omega\subset\mathbb{R}^2,\ z\in(-b(x,y),0)\subset\mathbb{R}\right\}, \tag{1}$$

Assuming irrotational motion, the velocity vector of the fluid is related to the scalar potential $\Phi(x,y,z;t):D\times(0,T]\to\mathbb{R}$ as

$$(u_x,u_y,u_z)^T=\nabla\Phi, \tag{2}$$

Where, for the temporal variable t, it is $t\in(0,T]$, $T\in\mathbb{R}_+$. In the following, the positive constant g denotes the acceleration of gravity. The initial boundary value problem (IBVP), for linear water wave propagation to be considered, is to find the water velocity potential $\Phi(x,y,z;t):D\times(0,T]\to\mathbb{R}^3$ and the water free surface elevation $\eta(x,y;t):\Omega\times(0,T]\to\mathbb{R}$ such that

$$\Delta\Phi=0, \text{ in } D, \text{ for all } t\in(0,T], \tag{3}$$

$$\nabla\Phi\cdot n_b=0, \text{ in } \Omega \text{ and } z=-b(x,y), \text{ for all } t\in(0,T], \tag{4}$$

$$g\eta+\frac{\partial\Phi}{\partial t}=0, \text{ in } \Omega \text{ and } z=0, \text{ for all } t\in(0,T] \text{ and} \tag{5}$$

$$\frac{\partial\eta}{\partial t}-\frac{\partial\Phi}{\partial z}=0, \text{ in } \Omega \text{ and } z=0, \text{ for all } t\in(0,T], \tag{6}$$

where n_b is the unit normal on $z=-b(x,y)$. Equation 3 represents the incompressibility of the fluid and irrotationality of the flow. Boundary condition 4 expresses the impermeability of the seabed. Eqs. 5 and 6, on the free surface, are the dynamic condition, i.e. force balance on the surface, and the fact that this is a material surface respectively.

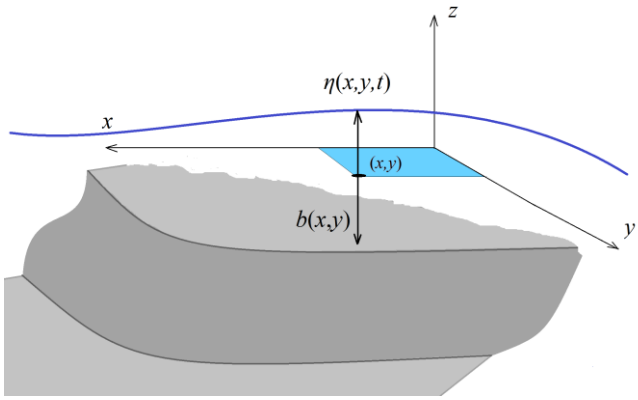

Fig 1. Water wave propagation over variable bathymetry region.

The above equation and boundary conditions are accompanied by appropriate initial conditions of the form

$$\Phi(x,y,z;t=0)=\Phi_o(x,y,z) \text{ and} \tag{7}$$

$$\eta(x,y,t=0)=\eta_o(x,y). \tag{8}$$

In the following analysis the value $\Phi_o=0$ will be exclusively used, while it will be assumed that $\eta_o\neq0$ only in the region $\Omega_o\subset\subset\Omega$. The maximum value of the temporal variable T will be always selected such that

$$\nabla\Phi\cdot n_{\partial\Omega}=0, \text{ on } \partial\Omega\times(-b(\partial\Omega),0), \text{ for all } t\in(0,T] \text{ and} \tag{9}$$

$$\eta=0, \text{ on } \partial\Omega, \text{ for all } t\in(0,T], \tag{10}$$

Published in the Proceedings of the International Offshore and Polar Engineering Conference
2016-January (pp.1363-1370)

where $n_{\partial\Omega}$ is the unit normal on the boundary of Ω. These specific selections guarantee that the propagating disturbance does not reach the boundary of domain Ω in the examined time interval. Thus the problem considered is actually an approximation of the Cauchy problem for linear water waves. In the case that $\partial\Omega$ simulates a vertical impermeable obstacle (e.g. a vertical cliff), Eq. 9 is still valid while Eq. 10 must be substituted by

$$|\nabla\eta| = 0 \text{, on } \partial\Omega . \tag{11}$$

These conditions now express full reflection on the vertical boundary if now T is such that the propagating pulses reach $\partial\Omega$.

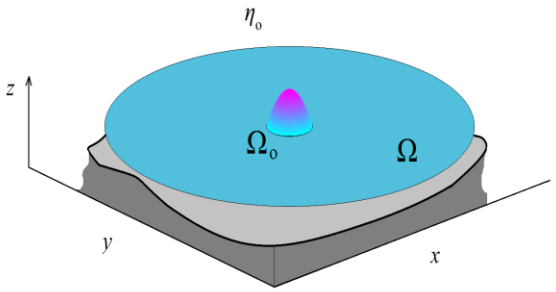

Fig 2. Initial condition for the free surface elevation.

Finally note that Eqs. 5~6, the conditions at $z = 0$ might be combined in a single equation for Φ, as

$$\frac{\partial^2\Phi}{\partial t^2} + g\frac{\partial\Phi}{\partial z} = 0 \text{, in } \Omega \text{ and } z = 0 \text{, for all } t \in (0,T] . \tag{12}$$

In the following section, a coupled mode system, equivalent to the above system of equations will be presented. The variational form of this coupled mode system will be the basis for the development of robust Finite elements for the numerical simulation of water wave propagation over variable bathymetry regions.

THE CONSISTENT COUPLED MODE SYSTEM

In the case of constant bathymetry, i.e. $b(x,y) = b = const$, the velocity potential might be represented in a series form as

$$\Phi(x,y,z;t) = \sum_{j=1}^{\infty} Z_j(z)\varphi_j(x,y;t) , \tag{13}$$

For the case of variable bathymetry, following (Belibassakis and Athanassoulis, 2006) an expansion of the velocity potential of the form

$$\Phi(x,y,z;t) = \sum_{j=1}^{\infty} Z_j(z;x,y)\varphi_j(x,y;t) , \tag{14}$$

is introduced. The subset of vertical modes $\{Z_n(z;x,y), n = 3,4,...\}$ is obtained by solving a Sturm-Liouville problem, formulated at the local vertical interval $-b(x) < z < \eta(x,t)$. This set contains both hyperbolic and trigonometric functions, dependent both on the local depth $h(x)$ and the (instantaneous) upper surface elevation $\eta(x,t)$. However, the boundary conditions satisfied by these local vertical eigenfunctions are not compatible with the boundary conditions of the problem at the bottom surface, if the bottom is not horizontal or mildly sloping, and at the upper surface. In order to overcome the mild-slope bottom approximation and to consistently satisfy the upper-surface boundary conditions, the present set has been enhanced by including the two additional modes $\{Z_1(z;x,y), Z_2(z;x,y)\}$ with unknown amplitudes $\{\varphi_1(x,t), \varphi_2(x,t)\}$.

The latter are the additional degrees of freedom required for the consistent satisfaction of the upper-surface and the sloping-bottom boundary conditions, respectively. The idea of the sloping-bottom mode has been presented by Athanassoulis & Belibassakis (1999) for the propagation of linearised waves in general bathymetry regions. The latter work has been extended to second-order Stokes waves (in the frequency domain) by Belibassakis & Athanassoulis (2002), where also the necessity of a free-surface additional mode has been discussed for the satisfaction of the (second-order) free-surface boundary condition. Accordingly, $\varphi_1(x,y;t)$ is termed the free-surface mode, $\varphi_2(x,y;t)$ the slopping bottom mode, $\varphi_3(x,y;t)$ is the propagating mode and $\varphi_j(x,y;t)$, $j = 4,5,...$ are evanescent modes.

Retaining only the free-surface, slopping bottom, the propagating and $m-1 \in \mathbb{N}$ evanescent nodes, an approximation of the wave potential is defined as

$$\hat{\Phi}(x,y,z;t) = \sum_{j=1}^{m+2} Z_j(z;x,y)\hat{\varphi}_j(x,y;t) . \tag{15}$$

Published in the Proceedings of the International Offshore and Polar Engineering Conference 2016-January (pp.1363-1370)

The governing Consistent Coupled Mode System (CCMS) is obtained by introducing expression (15) into Luke's functional,

$$\begin{aligned} \mathrm{I}(\bar{\Phi},\bar{\eta}) &= \mathrm{I}(\bar{\varphi}_1,\bar{\varphi}_2,...,\bar{\varphi}_{m+2},\bar{\eta}) \\ &= \rho\int_{t_1}^{t_2}\int_{\Omega}\int_{-b(x,y)}^{\bar{\eta}(x,y;t)}\left(\partial_t\bar{\Phi}+2^{-1}\left|\nabla\bar{\Phi}\right|^2+gz\right)dzdxdydt \end{aligned}, \quad (16)$$

considering the variational equations

$$\delta_\eta I(\bar{\varphi}_1,\bar{\varphi}_2,...,\bar{\varphi}_{m+2},\bar{\eta})=0\,, \quad (17a)$$

$$\delta_{\varphi_j} I(\bar{\varphi}_1,\bar{\varphi}_2,...,\bar{\varphi}_{m+2},\bar{\eta})=0\,,\ \ j=1,2,...,m+2 \quad (17b)$$

and retaining only the linear terms resulting in Eqs. 17. Adopting indicial notation with the standard summation convention (and dropping the hat from the approximations of η, φ_j for convenience), the CCMS finally reads

$$g\eta+\sum_{j=1}^{m+2}\frac{\partial\varphi_j}{\partial t}=0\,,\ \text{in}\ \Omega\,,\ \text{for all}\ t\in(0,T]\ \text{and} \quad (18)$$

$$\begin{aligned} &l_i\frac{\partial\eta}{\partial t}+a_{ij}(x,y)\left(\varphi_{j,xx}+\varphi_{j,yy}\right)+ \\ &\quad b_{ij(x)}(x,y)\varphi_{j,x}+b_{ij(y)}(x,y)\varphi_{j,y}+c_{ij}(x,y)\varphi_j=0 \end{aligned}, \quad (19)$$

in Ω, for all $t\in(0,T]$.

where $l_i=1$, $i=1,2,...,m+2$ and

$$a_{ij}(x,y)=\int_{-b(x,y)}^{0}Z_i(z;x,y)Z_j(z;x,y)dz\,, \quad (20a)$$

$$\begin{aligned} b_{ij(x)}(x,y) &= 2\int_{-b(x,y)}^{0}Z_i(z;x,y)Z_{j,x}(z;x,y)dz \\ &\quad +b_{,x}Z_i(-b)Z_j(-b) \end{aligned}, \quad (20b)$$

$$\begin{aligned} b_{ij(y)}(x,y) &= 2\int_{-b(x,y)}^{0}Z_i(z;x,y)Z_{j,y}(z;x,y)dz \\ &\quad +b_{,y}Z_i(-b)Z_j(-b) \end{aligned}, \quad (20c)$$

$$\begin{aligned} c_{ij}(x,y) &= \int_{-b(x,y)}^{0}Z_i(z;x,y)\Delta Z_j(z;x,y)dz \\ &\quad +\left[\left(b_{,x}Z_{j,x}+b_{,y}Z_{j,y}+Z_{j,z}\right)Z_i\right]_{z=-b}-\left[Z_{j,z}\right]_{z=0}. \end{aligned} \quad (20d)$$

The derivation and exact form of the local basis Z_j, with the additional free surface and slopping bottom mode has been presented formally and in detail by Belibassakis and Athanassoulis (2006). The interested reader is referred to the aforementioned study and the references therein.

VARIATIONAL FORM OF THE CCMS

Introducing the nondimensional variables

$$(\tilde{x},\tilde{y})=B^{-1}(x,y)\,,\ \tilde{t}=g^{1/2}B^{-1/2}t\ \text{and} \quad (21)$$

$$\tilde{\eta}=B^{-1}\eta\,,\ \tilde{\varphi}_j=g^{-1/2}B^{-3/2}\varphi_j\,, \quad (22)$$

where $B=\max_{(x,y)\in\Omega}|b(x,y)|$, the CCMS may be written (after dropping tildes for simplification), in the following nondimensional form

$$\eta+\sum_{j=1}^{m+2}\frac{\partial\varphi_j}{\partial t}=0\,,\ \text{in}\ \Omega_B\,,\ \text{for all}\ t\in(0,T_B]\ \text{and} \quad (23)$$

$$\begin{aligned} &l_i\frac{\partial\eta}{\partial t}+B^{-1}a_{ij}(Bx,By)\left(\varphi_{j,xx}+\varphi_{j,yy}\right)\neq \\ &+b_{ij(x)}(Bx,By)\varphi_{j,x}+b_{ij(y)}(Bx,By)\varphi_{j,y}+Bc_{ij}(Bx,By)\varphi_j=0 \\ &\quad\text{in}\ \Omega_B\,,\ \text{for all}\ t\in(0,T_B]. \end{aligned}, \quad (24)$$

where $T_B=g^{1/2}B^{-1/2}T$ and Ω_B is Ω scaled by a factor of B.

In the following, the standard notation $L^2(\Omega_B)$, $H^1(\Omega_B)$ will be used for the Lebesque square-integrable functions defined in Ω_B and the Lebesque square-integrable functions with square-integrable first derivatives respectively. For every Hilbert space W and $n\in\mathbb{N}$, the compound space W^n is defined as

$$W^n=\underbrace{W\times W\times.....\times W}_{n\ \text{times}}. \quad (25)$$

Multiplying Eq. 23 by $w\in L^2(\Omega_B)$, Eq. 24 by $v_i\in H^1(\Omega_B)^{m+2}$, applying the Green-Gauss theorem to the higher order term in Eq. (20), using the fact that $\varphi_{j,k}n_{\Omega_B k}=0$ for all $j=1,2,...,m+2$, $k=x,y$, and assuming sufficient regularity of the unknown fields, the variational equivalent of the presented problem is to find η, φ_j such that

Published in the Proceedings of the International Offshore and Polar Engineering Conference
2016-January (pp.1363-1370)

$$\iint_{\Omega_B} w\eta dxdy + \sum_{j=1}^{m+2} \iint_{\Omega_B} w \frac{\partial \varphi_j}{\partial t} dxdy = 0,$$
for all $w \in L^2(\Omega_B)$, a.e. in $(0,T_B]$ and (26)

$$\iint_{\Omega_B} l_i v_i \frac{\partial \eta}{\partial t} dxdy - B^{-1} \iint_{\Omega_B} a_{ij} v_{i,k} \varphi_{j,k} dxdy + \iint_{\Omega_B} (b_{ij(k)} - a_{ij,k}) v_i \varphi_{j,k} dxdy + B \iint_{\Omega_B} c_{ij} v_i \varphi_j dxdy = 0,$$
for all $v_i \in H^1(\Omega_B)^{m+2}$, a.e. in $(0,T_B]$. (27)

SEMI-DISCRETIZARION WITH LINEAR TRIANGLES

In this section, discretization of the variation form with linear triangle Finite Elements (FE) will be performed. Introducing a quasi-uniform triangulation $\mathbf{T}$ of the domain Ω_B and $u^h \in V^h \subset H^1(\Omega_B)$, such that for all $K \in \mathbf{T}$, the restriction of u^h in K satisfies

$$u^h\big|_K \in P^1(K),$$ (28)

where $P^1(K)$ is the set of all polynomials of degree at most one, defined in K, the discrete variational form reads

$$\iint_{\Omega_B} w^h \eta^h dxdy + \sum_{j=1}^{m+2} \iint_{\Omega_B} w^h \frac{\partial \varphi_j^h}{\partial t} dxdy = 0,$$
for all $w^h \in V^h \subset L^2(\Omega_B)$, a.e. in $(0,T]$ and (29)

$$\iint_{\Omega_B} l_i v_i^h \frac{\partial \eta^h}{\partial t} dxdy - B^{-1} \iint_{\Omega_B} a_{ij} v_{i,k}^h \varphi_{j,k}^h dxdy + \iint_{\Omega_B} (b_{ij(k)} - a_{ij,k}) v_i^h \varphi_{j,k}^h dxdy + B \iint_{\Omega_B} c_{ij} v_i^h \varphi_j^h dxdy = 0,$$
for all $v_i^h \in V_h^{m+2} \subset H^1(\Omega_B)^{m+2}$, a.e. in $(0,T]$. (30)

The system unknowns at node r, $r=1,2,3$ of element K are arranged in a vector U_r as

$$U_r = \left(\eta^r, \varphi_1^r, \varphi_2^r, ..., \varphi_m^r, \varphi_{m+1}^r, \varphi_{m+2}^r\right)^T.$$ (31)

Given the considered ansatz, the approximation of the unknown fields inside element K are denoted as

$$U^h\big|_K = \sum_{r=1}^{3} L_r U_r,$$ (32)

where, denoting $|K|$ the measure of K, the linear shape functions are

$$L_1(x,y) = \frac{1}{2|K|}\left[(x_2y_3 - x_3y_2) + (y_2 - y_3)x + (x_3 - x_2)y\right],$$ (33a)

$$L_2(x,y) = \frac{1}{2|K|}\left[(x_3y_1 - x_1y_3) + (y_3 - y_1)x + (x_1 - x_3)y\right],$$ (33b)

$$L_3(x,y) = \frac{1}{2|K|}\left[(x_1y_2 - x_2y_1) + (y_1 - y_2)x + (x_2 - x_1)y\right],$$ (33c)

where (x_r, y_r), $r=1,2,3$ are the coordinates of the vertices of K.

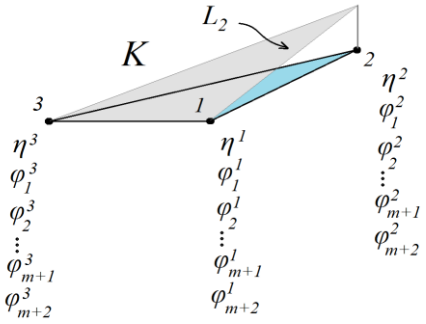

Fig 3. CCM-based Linear Triangle FEM and nodal degrees of freedom. One of the three shape functions is plotted.

Introducing the compound vector of nodal unknowns

$$\mathbf{U}_K = \left(U_1^T, U_2^T, U_3^T\right)^T$$, it is (34)

$$U^h\big|_K = \mathbf{N}\mathbf{U}_K$$, with $\mathbf{N}_{(m+3)\times(3m+9)} = \left[L_1\mathbf{I}_{m+3} \quad L_2\mathbf{I}_{m+3} \quad L_3\mathbf{I}_{m+3}\right]$, (35)

where $\mathbf{I}_{m+3}$ is the unit matrix of dimension $m+3$.
Inserting form (35) into the restriction of the discrete variational form (29)-(30) into element K, the matrix element equation

$$\mathbf{M}_K \frac{d\mathbf{U}_K}{dt} + \mathbf{K}_K \mathbf{U}_K = 0_{(m+3)\times 1},$$ (36)

is obtained. In Eq. (36) it is

$$\mathbf{M}_K = \iint_K \mathbf{N}^T \mathbf{m} \mathbf{N} dxdy,$$ (37a)

Published in the Proceedings of the International Offshore and Polar Engineering Conference
2016-January (pp.1363-1370)

$$\mathbf{K}_K = \iint_K \left(\mathbf{N}_{,x}^T \mathbf{a} \mathbf{N}_{,x} + \mathbf{N}_{,y}^T \mathbf{a} \mathbf{N}_{,y}\right) dxdy + \iint_K \left(\mathbf{N}^T \mathbf{b_x} \mathbf{N}_{,x} + \mathbf{N}^T \mathbf{b_y} \mathbf{N}_{,y}\right) dxdy + \iint_K \mathbf{N}^T \mathbf{c} \mathbf{N} dxdy \quad , \tag{37b}$$

where

$$\mathbf{m} = \begin{bmatrix} 0 & l_{1\times(m+2)} \\ l_{(m+2)\times 1} & \mathbf{0}_{m+2} \end{bmatrix}, \ \mathbf{a} = \begin{bmatrix} 0 & 0_{1\times(m+2)} \\ 0_{(m+2)\times 1} & B^{-1}a_{ij} \end{bmatrix},$$

$$\mathbf{b_x} = \begin{bmatrix} 0 & 0_{1\times(m+2)} \\ 0_{(m+2)\times 1} & b_{ij(x)} - B^{-1}a_{ij,x} \end{bmatrix},$$

$$\mathbf{b_y} = \begin{bmatrix} 0 & 0_{1\times(m+2)} \\ 0_{(m+2)\times 1} & b_{ij(y)} - B^{-1}a_{ij,y} \end{bmatrix},$$

$$\mathbf{c} = \begin{bmatrix} 1 & 0_{1\times(m+2)} \\ 0_{(m+2)\times 1} & Bc_{ij} \end{bmatrix}.$$

IMPLEMENTATION AND TIME INTEGRATION

Implementation issues of the proposed Finite Element (FE) scheme and numerical time integration of the resulting system of Ordinary Differential Equations (ODEs) will be the subjects of this section.

Implementation Issues of the FE scheme

The calculation of the element matrix equation, Eq. (36), involves the computation of several surface integrals as dictated by Eqs.37. These integrals will be approximated by the Gaussian Quadrature of degree 1 as

$$\mathbf{M}_K \approx \frac{1}{2}|K|\mathbf{N}^T(x_m, y_m)\mathbf{m}(x_m, y_m)\mathbf{N}(x_m, y_m)\,. \tag{38a}$$

$$\mathbf{K}_K \approx \frac{1}{2}|K|\left(\mathbf{N}_{,x}^T\mathbf{a}(x_m, y_m)\mathbf{N}_{,x} + \mathbf{N}_{,y}^T\mathbf{a}(x_m, y_m)\mathbf{N}_{,y}\right) + \frac{1}{2}|K|\mathbf{N}^T(x_m, y_m)\left(\mathbf{b_x}(x_m, y_m)\mathbf{N}_{,x} + \mathbf{b_y}(x_m, y_m)\mathbf{N}_{,y}\right). + \frac{1}{2}|K|\mathbf{N}^T(x_m, y_m)\mathbf{c}(x_m, y_m)\mathbf{N}(x_m, y_m) \tag{38b}$$

where

$$(x_m, y_m) = \frac{1}{3}\left(\sum_{r=1}^{3} x_r, \sum_{r=1}^{3} y_r\right),$$

are the coordinates of the barycenter of K.

Assembly of the element contributions expressed through matrix Eq. 36 for all $K \in \mathbf{T}$ yields a system of ODEs of the form

$$\mathbf{M}\frac{d\mathbf{U}}{dt} + \mathbf{K}\mathbf{U} = \mathbf{0}\,. \tag{39}$$

Numerical time integration of the above system will be the subject of the subsequent paragraph.

Time Integration of the FEM system

For $N_t \in \mathbb{N}$ the number of time increments and a constant step size $\tau = T_B / N_t$, a uniform partition of $[0, T_B]$ having the form

$$0 = t_1 < t_2 < \ldots < t_{N_t} < t_{N_t+1} = T_B\,,$$

is defined. For the time integration of the ODE system defined in Eq. 39, the Crank-Nicolson scheme is adopted. Given the initial value $\mathbf{U}^1 = \mathbf{U}(0) = \mathbf{U}_o(\eta_o^h)$, the solution update is

$$\mathbf{U}^{n+1} = \left(\mathbf{M} + \frac{1}{2}\tau\mathbf{K}\right)^{-1}\left(\mathbf{M} - \frac{1}{2}\tau\mathbf{K}\right)\mathbf{U}^n, \tag{40}$$

for $n = 1, 2, 3, \ldots, N_t$.

NUMERICAL RESULTS AND DISCUSSION

The CCMS-based 3-node triangle for linear water wave propagation in variable bathymetry domains has been implemented in MATLAB. In this section, the proposed numerical scheme is applied to the simulation of an initial free-surface disturbance propagation. The initial elevation has the form of a Gaussian distribution, i.e.

$$\eta_o(x, y) = A_c \exp\left(-f^2(x^2 + y^2)\right) \ \text{m}\ , \tag{41}$$

inside the domain $x^2 + y^2 < R_c$, and is zero if $x^2 + y^2 > R_c$. The bathymetry is selected so as to represent a shoaling topography with respect to the spatial variable x, uniformly with respect to y. The particular form

Published in the Proceedings of the International Offshore and Polar Engineering Conference
2016-January (pp.1363-1370)

$$b(x,y) = 4 - 2\tanh(0.1x) \quad \text{m}\,, \tag{42}$$

has been adopted. In that manner, the water depth ranges smoothly between the values $2\,\text{m}$ and $6\,\text{m}$. In order for the linear theory to apply, we select $A_c = 0.3\,\text{m}$ and thus $A_c / B = 0.3/6 = 0.05 << 1$. Radius R_c is set to $R_c = 15\,m$ so that the non-dimensional diameter of the initial pulse is 30/6=5 a value in the intermediate depth range. Finally the value $f^2 = 0.075$ is selected, while the initial value of the velocity potential is zero. This value ensures that the initial disturbance is practically zero just before $x^2 + y^2 = R_c$.

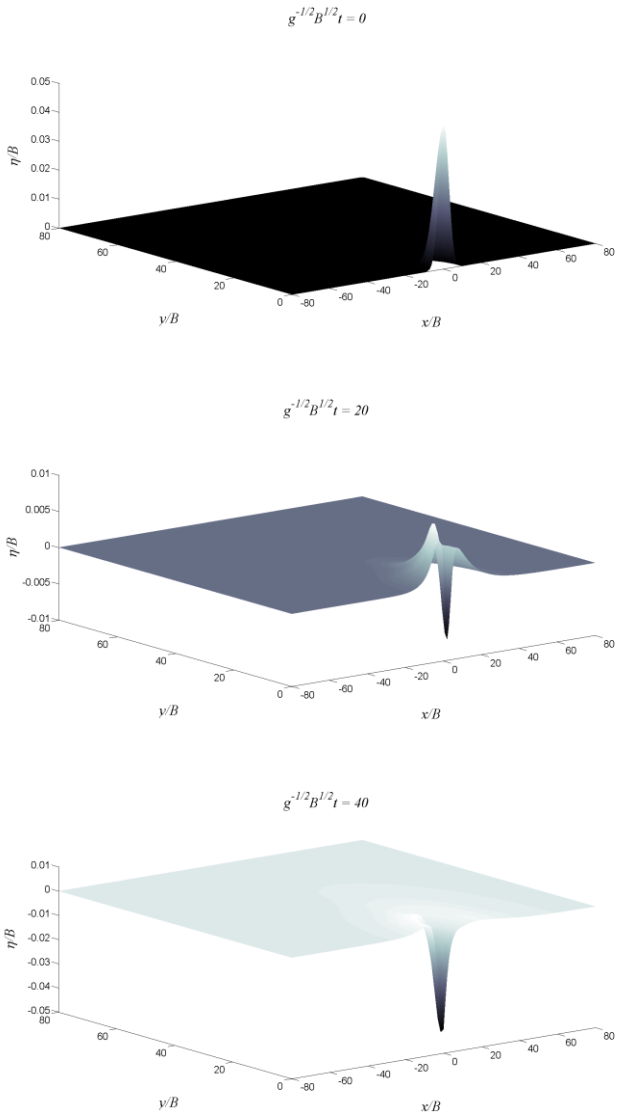

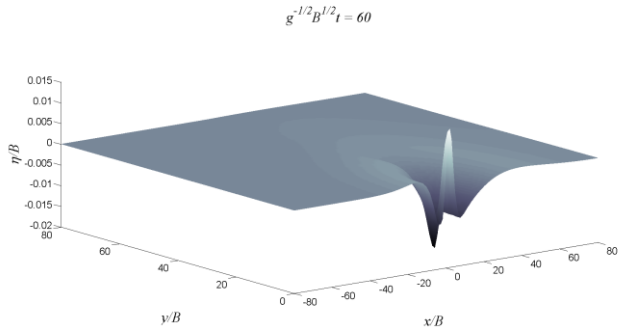

Fig 4. Snap-shots of the free surface elevation at nondimensional time instances 0, 20, 40, 60. The first plot corresponds to the selected initial condition. Due to the symmetry with respect to the x axis, the solution domain is a subset of the upper half-plane.

The IBVp of the propagating pulse has been solved with a sequence of three mesh refinements termed henceforth MESH I, MESH II and MESH III. Due to the symmetry of the domain and initial condition with respect to the x axis, only half of it needs to be discretized. In this particular example, domain Ω_B is the rectangle $[-80, 80]\times[0, 80]$. The maximum time step used is $\tau = 0.5$. MESH I consists of 2736 Triangles and 1435 nodes. MESH II contains a total of 10944 Triangles and 5605 nodes. Finally, MESH III, has 43.774 elements and 22.153 nodes. Solutions with an increasing number of modes have been obtained until convergence has been established. A total of five to six modes have been found to be adequate for convergence.

Figure 4 presents function η at three different nondimensional time instances, namely $g^{1/2}B^{-1/2}t = 0, 20, 40, 60$. The first of these values corresponds to the η_o / B distribution along Ω_B. The pulse propagates faster along the positive x axis, which is to be expected since the depth increases towards this direction. Towards the opposite direction, the pulse propagation is slower and the amplitude of the waveform increases due to shoaling. These phenomena are more evident in Figure 5, where the time profile of the pulse at three different locations along the x axis is plotter. The first diagram corresponds to the coordinates $(x/B, y/B) = (0,0)$. The second and third diagrams correspond to $(x/B, y/B) = (-15,0)$ and $(x/B, y/B) = (15,0)$, respectively. In these coordinates the time profile of the waves generated by the propagation of the same initial disturbance over constant bathymetry $b = 6\,\text{m}$ are also plotted.

Published in the Proceedings of the International Offshore and Polar Engineering Conference
2016-January (pp.1363-1370)

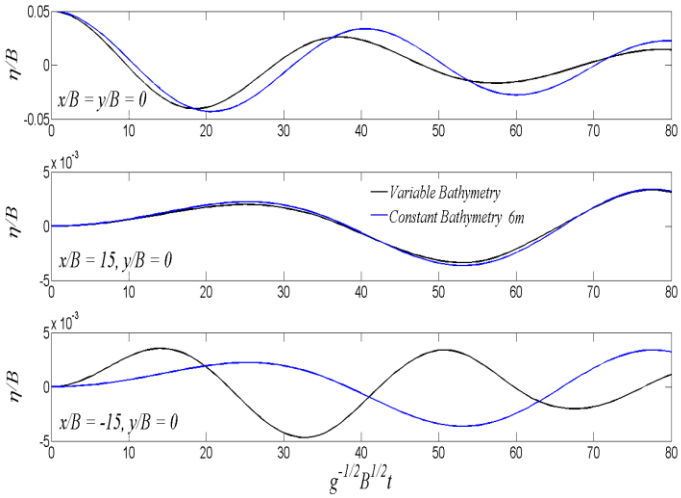

Figure 5. Time profile of the wave field at three different locations along the x axis. The solution corresponding to propagation over constant depth (6 m) is also plotted.

The effect of shoaling in also depicted in figures 6, 7, 8, 9. In Figures 6, 7 the upper surface elevation for nondimensional time 25 and 50 is plotted. Figures 8 and 9 are the contours of η / B, corresponding to the upper surface elevation of figure 6 and figure 7 respectively. The contours of the same pulse propagating over constant depth 6 m is plotted with a gray line. These contours are circles due to the axial symmetry of the particular problem for constant bathymetry. Lower propagation speed in shallower water makes the respective contours for the variable bathymetry case distorted.

Figure 10 demonstrates the performance of the present numerical procedure. A comparison of the solution quality for the three meshes is carried out by comparing the free surface elevation time profile at three locations along the x axis.

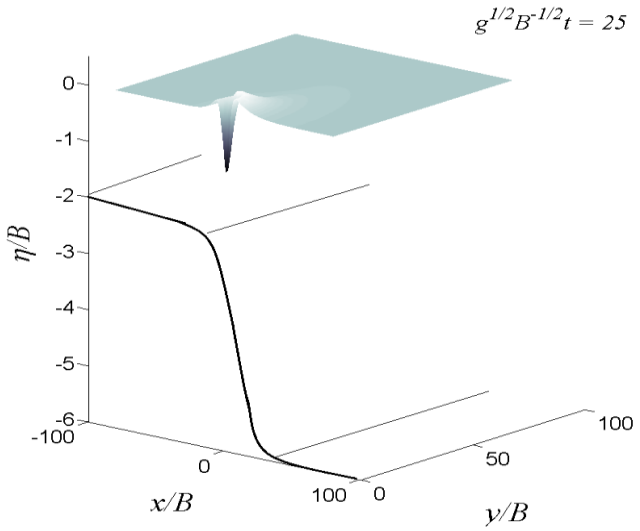

Fig 6. Upper surface elevation at nondimensional time 25 and the seabed profile defined by Eq. 41. The upper surface elevation is multiplied by a factor of 50.

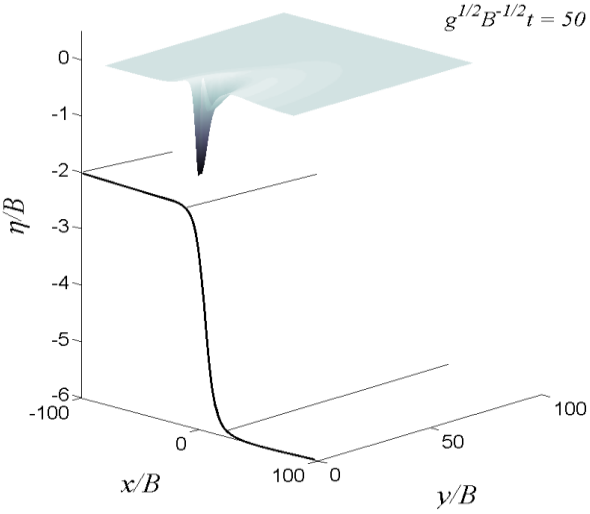

Fig 7. Upper surface elevation at nondimensional time 50 and the seabed profile defined by Eq. 41. The upper surface elevation is multiplied by a factor of 50.

The three lines in figure 10, depict the free surface elevation time profile at the coordinates $(x/B, y/B) = (0,0)$, $(x/B, y/B) = (15,0)$ and $(x/B, y/B) = (-15,0)$ respectively. Each plot contains three curves associated to the solution obtained by the triangulations MESH I, MESH II, MESH III. Error

Published in the Proceedings of the International Offshore and Polar Engineering Conference
2016-January (pp.1363-1370)

reduction is observed when finer discretization is adopted. Figure 11 is a plot of the error indicator

$$\mathrm{Er}(x_o / B, y_o / B) = \max_j \left| \eta(x_o / B, y_o / B t_j) - \eta_e(x_o / B, y_o / B, t_j) \right|, \quad (43)$$

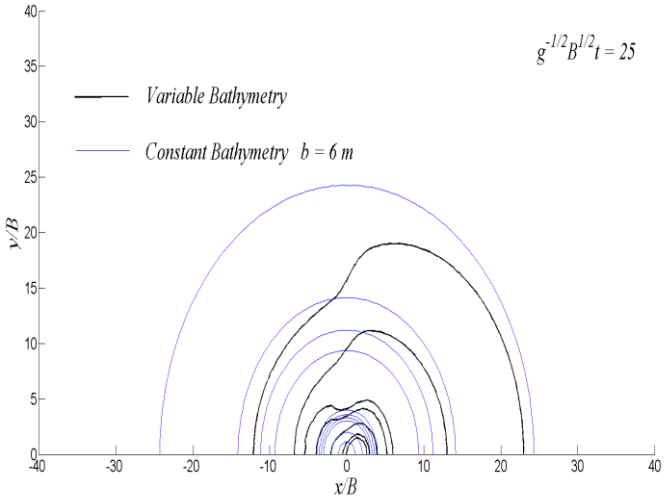

Fig 8. Contour of the upper-surface elevation corresponding to figure 6. Isoclines of the free surface elevation in the case of constant bathymetry 6 m are also plotted (thin blue line).

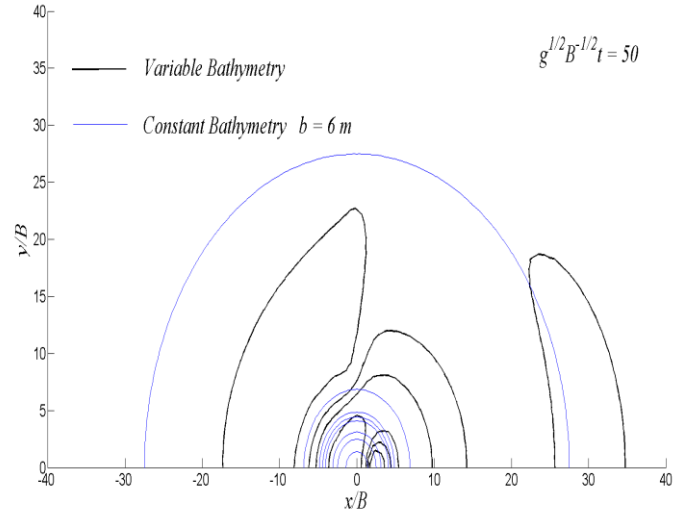

Figure 9. Contour of the upper-surface elevation corresponding to figure 7. Isoclines of the free surface elevation in the case of constant bathymetry 6 m are also plotted (thin blue line).

where η_e is a reference solution obtained with a finer mesh (MESH IV) consisting of 89190 elements and 45016 nodes. The first point in Figure 11 corresponds to a very coarse mesh of 684 elements and 376 nodes. The other points correspond to meshes MESH I, MESH II and MESH III.

The method described can be easily applied to the construction of higher order Lagrange Elements for linear water wave propagation. It is also worth mentioning that the presented procedure constitutes the basis for the development of similar techniques for the solution of nonlinear water wave propagation problems.

CONCLUSIONS

A robust Finite Element procedure for the numerical simulation of transient, linear water wave propagation over variable bathymetry regions is presented. The method utilises a coupled mode system based on an enhanced series expansion of the water wave potential introduced by Belibassakis & Athanassoulis (2006, 2011). The solution of the weak form of this rapidly convergent Coupled Mode System is realised with the Finite Element Method. Linear triangles are employed and time integration of the resulting system of ordinary differential equations is performed by means of the Crank-Nicolson scheme. The proposed solution strategy is applied to the study of the propagation of an initial disturbance at the free surface. The good performance of the method is demonstrated and the transient motion of the free surface interacting with shoaling seabed topography is analysed.

Published in the Proceedings of the International Offshore and Polar Engineering Conference
2016-January (pp.1363-1370)

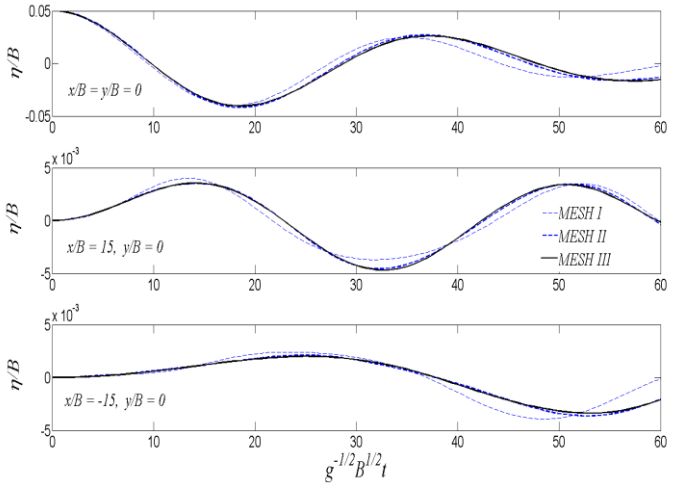

Fig 10. Performance of the FEM solution at three different nodes for quasi-unifrom mesh refinement.

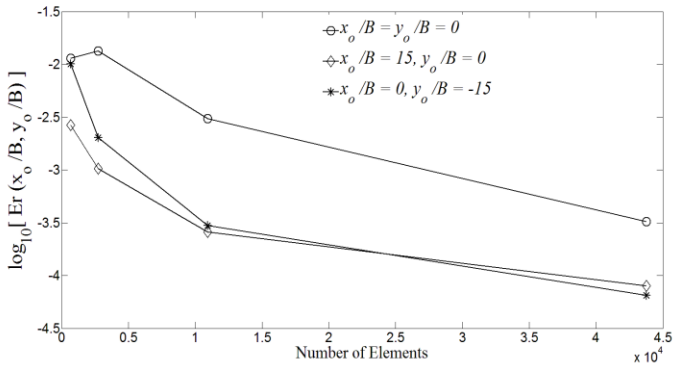

Fig 11. Plot of the error indicator Er at three different nodes for quasi-uniform mesh refinement, as a function of the number of elements employed.

REFERENCES

- Athanassoulis, GA, and Belibassakis KA (1999). "A consistent coupled-mode theory for the propagation of small amplitude water waves over variable bathymetry regions", *J Fluid Mech*, 389, 275-301.
- Belibassakis, KA, and Athanassoulis, GA (2002). "Extension of second-order Stokes theory to variable bathymetry", *J Fluid Mech*, 464, 35-80.
- Belibassakis, KA, and Athanassoulis, GA (2006). "A coupled-mode technique for weakly nonlinear wave interaction with large floating structures lying over variable bathymetry regions", *Appl Ocean Res*, 28, 59-76.
- Belibassakis, KA, Gerostathis, ThP, and Athanassoulis, GA (2011). "A coupled-mode for water wave scattering by horizontal, non-homogeneous current in general bottom topography", *Appl Ocean Res*, 33, 384-397.
- Dingemans, M (1997). *Water Wave propagation over uneven bottoms*, World Scientific.
- Kardestuncer, H (ed) (1987). *Finite element handbook*, Mcgraw-Hill.
- Madsen, PA, Fuhrman, DR, and Wang B (2006). "A Boussinnesq-type method for fully nonlinear waves interacting with rapidly varying bathymetry", *Coast Eng*, 53(5-6), 487-504.
- Massel, S (1993). "Extended refraction-diffraction equations for surface waves", *Coast Eng*, 19, 97-126.
- Stoker, JJ (1957). *Water Waves The Mathematical Theory with Applications*, Interscience Publishers Inc., New York.